Monte Carlo evaluation of a CZT 3D spectrometer suitable for a Hard X- and soft-γ rays polarimetry balloon borne experiment

E. Caroli, G. De Cesare, R. M. Curado da Silva, L. Abbene, N. Auricchio, C. Budtz-Jørgensen, S. Del Sordo, P. Ferrando, J. L. Galvèz, M. Hernanz, J. Isern, I. Kuvvetli, P. Laurent, O. Limousin, J. M. Maia, M. Moita, N. Produit, J. B. Stephen, A. Zappettini

***Abstract*– Today, the measurement of the polarization status of cosmic sources high-energy emission, is recognized as a key observational parameter to understand the active production mechanism and its geometry. Therefore, a mandatory requirement for new instrumentations operating in this energy range will be to provide high sensitivity for polarimetric measurements. In this framework, we have presented the concept of a small high-performance imaging spectrometer optimized for polarimetry between 100 and 600 keV suitable for a stratospheric balloon-borne payload and as a pathfinder for a future satellite mission. The detector with 3D spatial resolution is based on a CZT spectrometer in a highly segmented configuration designed to operate simultaneously as a high performance scattering polarimeter. Herein, we report results of a Monte Carlo study devoted to optimize the configuration of the detector for polarimetry with particular focus on event selection filter able to increase the polarimetric performance. This preliminary analysis shows that a procedure to optimize the polarization response of a 3D spectrometers should first of all determine the best tradeoff between the statistical significance and the quality of the modulation factor.**

I. Introduction

THE measurements of the polarization status of hard X- and soft γ-rays from cosmic sources represent a powerful diagnostic tool to identify the emission mechanisms and to obtain fundamental information on the geometry of emitting region [1]. To date very few reliable polarization measurements in the hard X-/soft gamma-ray domain are available. Significant results were recently obtained for a very long exposure (>10^6 s) using the SPI (SPectrometer on INTEGRAL) and IBIS (Imager on-Board INTEGRAL Satellite) telescopes on the polarization of the Crab (that is the most intense source in this energy domain) [2, 3] and on Cyg-X-1 [4]. Furthermore, the signature of polarisation have been observed in some strong Gamma-Ray Burst [5, 6]. Many different research groups are involved in the development of hard X- and soft gamma-ray polarimeters for balloon experiments and/or for space instrumentation; see for some examples [7, 8, and 9]. Recently, the data obtained by the PoGOLite balloon flown in July 2013 on the Crab are in good agreement with the SPI rsults in a different energy range [10].

Herein we present some undergoing activities for the design of a balloon borne experiment based on a compact highly CZT segmented detector dedicated in particular to assess its capability as a scattering polarimeter in the 60-600 keV range through the measurement of the Crab pulsar polarisation. The Compact μ-Spectrometer for Polarimetry (CμSP), we propose, can be considered also as the pathfinder for high performance focal plane detector in future space mission based on new high focusing optics [11, 12].

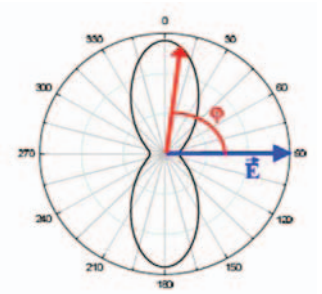

Fig. 1. The K-S scattering probability diagram for polarized photons vs the azimuthal angle (φ) for 90° scattering angle. The vector E gives the direction of the photons polarization plane.

II. Scattering Polarimetry with Pixel Detectors

In the hard X- and soft γ-rays regime polarimetric measurements are possible using Compton scattered events. The Klein-Nishina (K-N) equation cross-section exhibits an azimuthal dependency in the scattering direction for linearly polarized photons [13]; for polarized photons, the probability

Manuscript received .....

E. Caroli, G. De Cesare, N. Auricchio, and J. B. Stephen are with INAF/IASF-Bologna, Via Gobetti 101, I-40129 Bologna, Italy (phone: +390516398678, e-mail: caroli @iasfbo.inaf.it).

R. M. Curado da Silva, J. M. Maia, and M. Moita are with LIP, Dep. de Física, Universidade de Coimbra, P-3004-516 Coimbra, Portugal (phone: +351239410663 , e-mail: rui.silva@coimbra.lip.pt).

L. Abbene is with the DiFC, University of Palermo, Via Archirafi n. 36, I-90123 Palermo, Italy (telephone: +3909123899081, e-mail: leonardo.abbene@unipa.it)

C. Budtz-Jørgensen, and I. Kuvvetli are with DTU Space, DK-2800 Kgs. Lyngby, Denmark (phone: +4545259726, e-mail: carl@space.dtu.dk).

S. Del Sordo is with INAF/IASF-Palermo, Via Ugo La Malfa 153, I-90146 Palermo (Italy) (phone: +390916809563; e-mail: delsordo@ifc.inaf.it)

P. Ferrando, P. Laurent, and O. Limousin are with CEA Saclay, DSM/Irfu/Service d'Astrophysique, L'orme des merisiers, F-91191 Gif-sur-Yvette Cedex, France (phone: +33169086294; e-mail: olivier.limousin@cea.fr).

J. L. Galvèz, M. Hernanz, and J. Isern are with ICE-CSIC/IEEC, Campus UAB, E-08193 Bellaterra, Spain (phone: +34935814356; e-mail: Hernanz@ieec.uab.es).

N. Produit is with ISDC Data Centre for Astrophysics, University of Geneva, CH-1290 Versoix, Switzerland (phone: +41223792140, e-mail: Nicolas.Produit@unige.ch)

A. Zappettini is with CNR/IMEM, Parco Area delle Scienze 37/A, I-43124 Parma, Italy (phone: +390521269296, e-mail: zapp@imem.cnr.it)

distribution of the scattering angle will present a maximum along the direction orthogonal to the polarisation plane and a minimum in the parallel one (Fig. 1).

A pixel (i.e., a highly segmented) detector offers an efficient method to measure the linear polarisation status of incoming photons using Compton scattering. Indeed, with a coincidence event logic, each element/pixel can act at the same time as both a scattering and a detection unit. A further advantage being that the polarimetric measurement can performed in parallel with all the other standard operational modes (i.e. imaging, spectroscopy and timing). In the last fifteen years, we performed different experiments on CdTe/CZT pixel detectors at the ESRF (Grenoble) with the linearly polarized high-energy beam at ID15 [14, 15, 16, and 17].

For a pixel detector, a simple figure of merit as scattering polarimeter, the Q factor, is defined by:

$$Q = \frac{N_x - N_y}{N_x + N_y} \quad (1)$$

where N_x and N_y are the sums of scattered events in two orthogonal directions. In fact, Q is a periodical (= 2π) function of the azimuthal angle φ. The Q reaches a maximum in absolute value when one of the two orthogonal directions is parallel to the polarized photon electric field direction.

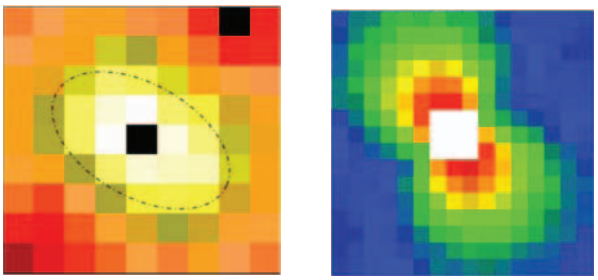

Fig. 2. Scatter maps of a 98% polarized beam collimated into one of the center pixels with the polarization direction inclined 45° with respect to detector sides: (left) 5 mm thick CZT detector (POLCA) with 11×11 pixels of 2.5 mm pitch. (right) Caliste module equipped with 2 mm thick CZT pixel spectrometer (16×16 pixels with 0.625 mm pitch).

In such type of detectors, the polarization status of the incoming flux can be evaluated by building the distribution of the two interaction positions, depositing E_1 and E_2 respectively. Fig. 2 shows two examples of reconstructed scattering maps obtained with two different CZT pixel detectors.

III. 3D CZT/CdTe Spectrometers for Scattering Polarimetry

The performance of a polarimeter based on a highly segmented detector is strongly dependent on its geometrical configuration. To achieve good polarimetric performance for hard X/soft γ rays, the detector should fulfil the following requirements:

- high scattering efficiency, achievable with increased thickness;
- high modulation factor achievable with decreased thickness and pixel size;
- fine spectroscopy allowing effective background rejection and good event selection.

An efficient answer to all this requirements is offered by spectro-imagers with three dimension spatial resolution (3D spectrometers). In particular, concerning CZT/CdTe detector technology, at least two different solutions are under study. Both are based on the PTF (Planar Transverse Field) irradiation configuration (Fig. 3), in which the photon absorption thickness is independent from the charge collecting distance, practically limited only by bulk crystal growing technology.

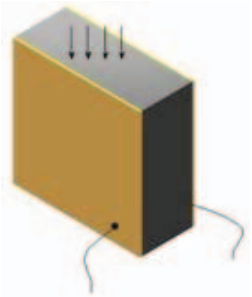

Fig. 3. PTF irradiation configuration: the photons are impinging onto the detector orthogonally to the collecting field direction

The first solution (a) use pixel spectrometer as basic sensor unit (Fig. 4a). This configuration is under development by the ICE group in Bellaterra [18]. The second solution (b) is under development at the DTU-Space, IASF/INAF and IMEM/CNR [19-20]. In this case, the sensor unit is a bulk CZT crystal with both the electrode sides segmented in two sets of orthogonal micro-strips (Fig. 4b). Furthermore, the anode side set implement a drift strip configuration allowing the evaluation of the photon interaction position between the two electrode sides.

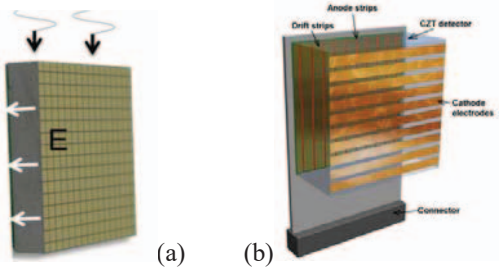

(a) (b)

Fig. 4. (a) Pixel detector used in PTF. The basic unit is a single 12.5×12.5 mm2 CdTe crystal (2 mm thick) with a planar cathode and with the anode segmented in a 11×11 pixel array with 1 mm pitch. (b) Drift strip detector used in PTF. The basic unit is a single 20×20 mm^2 CZT crystal (5 mm thick).

CZT/CdTe sensors units, regardless of the configuration, can be assembled on thin insulating supports to build linear modules. Therefore, the linear modules itself could be stacked together as in the scheme shown in Fig. 5.

We point out that such type of 3D detector modules is equivalent to stack of thinner layers, but without any passive material within.

The final size of 3D pixels (i.e. voxels) in these modules depends on both the configuration and the segmentation of electrodes the CdTe/CZT sensors units and can range between mm and hundreds of micrometers scales.

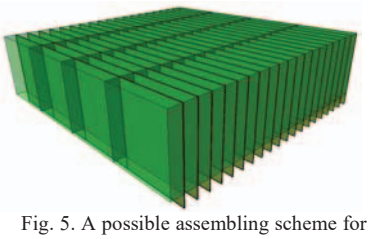

Fig. 5. A possible assembling scheme for a 3D stack module.

IV. The CμSP Balloon Borne Payload Outline

In order to realize the detector of CμSP, we propose to build a mosaic of 2×2 of the above 3D stack modules. Each module will be rotated 90° with respect to the adjacent ones to minimize the systematic effect on the polarization modulation induced by the voxel geometry (e.g. voxel dimensions asymmetry, diagonal effect) [17]. Table I reports the main characteristics of possible configuration for the CμSP detector.

The detector is coupled with a simple (i.e. same size of the detector) Coded Mask made by thin high Z opaque elements to provide imaging up ~100 keV. The imaging (at 20′ level) will be used to control the source pointing and the calibration of the instrument itself. In the opposite, the mask shall become almost completely transparent above ~150 keV to expose the full sensitive detector area, increasing the polarization sensitivity.

The main objective of the CμSP balloon payload will be to assess definitively the performance of highly segmented high Z 3D spectrometers as scattering polarimeters by performing a measurement of the Crab source in the range between 100-600 keV. The success of such balloon experiment will confirm the advantages and the suitability of using this type of detector for future space mission based on new high energy focusing systems.

Table I. CμSP Detector Main Characteristics and Resources. (a) and (b) refers to PTF pixel and PTF drift strip sensor units, respectively.

Sensitive area	400 cm^2
3D configuration	2×2 mosaic of stack modules
Stack module	20 linear module (10×10 cm^2)
Linear module	4 CZT (2 mm thick) crystals
CZT/CdTe unit	2.5×2 cm^2, 5 mm thick
Voxel size	2×2×2 mm^3 (geometric)
Voxels number	~30000 (a)/15000 (b)
Power (AFEE)	~40 (a)/~20 (b) W
Active Weight	~1.5 kg
Instrument type	Simple Coded Mask
Mask-Detector Separation	100 cm
Shielding	Passive
Detector Operative Range	5-600 keV
Polarimetry Range	100-600 keV

The main objective of the CμSP balloon payload will be to assess definitively the performance of highly segmented high Z 3D spectrometers as scattering polarimeters by performing a measurement of the Crab source in the range between 100-600 keV. The success of such balloon experiment will confirm the advantages and the suitability of using this type of detector for future space mission based on new high energy focusing systems.

A measure of the polarimetric capability of an instrument is given by the Minimum Detectable Polarization ($MDP_{99\%}$) defined as [1]:

$$MDP_{99\%} = \frac{4.29}{A \cdot \varepsilon \cdot S_F \cdot Q_{100}} \sqrt{\frac{A \cdot \varepsilon \cdot S_F + B}{T}} \qquad (2)$$

Based on the chosen detector configuration and on the Q values (0.3-0.5) obtained with CZT pixel prototype in the different experiments at the ESRF (Grenoble), we expect to achieve with the CuSP instrument a MDP level between 2 and 5% for a 10000 s observations over the range 60-600 keV [21].

V. Monte Carlo Study of the Polarimetric 3D Detector Response

Monte Carlo modelling represents an essential step in the optimisation of pixel detector polarimetric response and in defining the best trade-off between performance and detector design complexity. Using GEANT4 [22], we are performing numerical simulations using a simple model based on a CZT block (20 cm × 20 cm × 2 cm) that can be segmented in 3D at any defined voxel size by a SW tool developed in MATLAB [23]. This tool read the event files generated by GEANT4 simulation runs and allow to perform and implement different analysis by an easy parametrisation of different parameters.

The simulations, related to the present work, are based on the following characteristics for both the detector and the impinging photon flux:

- Parallel and on axis flux (incidence angle=0°) impinging uniformly on the overall detector top surface (400 cm^2);
- Impinging flux 100% linearly polarized;
- Photons spectrum: $10 \times E^{-2}$ photons/keV/cm^2/s in the 60-600 keV range (Crab like spectrum) for a total of 10^6 photons;
- Segmentation of the detector volume: 2 mm × 2 mm × 2 mm voxels.
- Detector volume equivalent to a 3D (i, j, k) array of 100×100×20 elements.

The simulated number of photons is equivalent to a source observation time of ~4.6 hours. This time is fully compatible with the typical length of an observation pointed to the Crab source from a mid-latitude balloon borne experiment launched in the northern hemisphere.

Table II report the values of double events efficiency in 4 evenly spaced logarithmic energy band between 60 and 600 keV together with the modulation factor Q obtained using Eq. (1) by summing the counts over the central row and the central column of the scattering map. This draft evaluation of Q is possible because we know the orientation of the polarization vector of the imping photons. Both double event efficiencies and the Q values are given the first time considering all the double events (*Z=free*) and in the second case counting only double events in which each hits have the same Z coordinate (*Z=cost*). This selection tend to increase the Q factor because is equivalent to select scattering angle in average more close to 90°.

Table II. Double events efficiency and relative modulation factor Q

ΔE (keV)	**Double *Z=free***	**Q_{free}**	**Double *Z=cost***	**Q_{cost}**
60-107	0.6%	0.22	0.5%	0.24
107-190	7.9%	0.30	3.9%	0.31
190-337	22.9%	0.19	7.5%	0.33
337-600	23.1%	0.19	6.1%	0.30

In general, with 2 mm segmentation scale in 3D, the selection of double events with *Z=cost* allow a small improvement of the Q factor in almost all energy bands. However, this selection is

paid by strong loss in statistics due to the decrease of double events efficiency: from 1/2 to more than 1/3 of all double events. In fact, the small improvement in Q does not compensate the reduction of the double event detection efficiency (ε) because the detection efficiency and the Q value weight as $1/(Q \times sqrt(\varepsilon))$ in defining the MDP (Eq. 2).

Using the results reported in Table II, we concentrated our analysis in the third energy band, in which the double events efficiency maximizes together with the raw evaluated Q factor. This energy band represent just the 15% of the total impinging photons. We use these energy band to mainly study the effect in the modulation factor evaluation of event filters based on the distance between the two hits (named in the following also adjacency). Fig. 6 (left) show the histogram of the double event hits distribution distance in pixels in the band 190-337 keV. From this figure is clear that the first order adjacency (i.e. the two hits happens in adjacent pixels) is dominant, and that distance larger than 5-6 are really few.

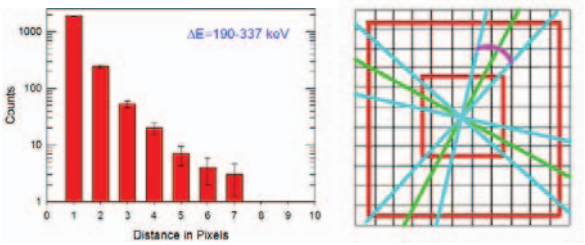

Fig. 6. (left) Distance distribution between the hits of double events in the third energy band of Table II; (right) The counts integration scheme used to build the modulation curves. The cyan (light) lines limit the two orthogonal angular sectors used to calculate the sums of scattered events in two orthogonal directions (N_x and N_y) required by Eq (1). The red (dark) square concentric perimeters exemplify the applied adjacency filter.

Fig. 6 (right) shows the method implemented in the MATLAB data analysis tool to build the modulation curve. The two orthogonal angular sector (0.2° aperture) are rotated by a defined angular step (10° in the present work) to cover 360°. Therefore, for each phase angle the modulation factor Q(α) is evaluated by using Eq (1). The results of this procedure all the double events recorded in the energy band 190-337 keV is plotted in Fig. 7 for the two cases: double events with *Z=free* and *Z=cost*, respectively.

The shapes of both modulation curves in Fig. 7 exhibit a quite evident large scale discretization with the phase angle. This is the effect of the first order adjacency counts that are dominant in the statistics. The scattering in the first order adjacency pixel tend to limits the phase angle sensitivity to 40° (i.e. 360/9 surrounding pixels) steps.

In order to overcome this effect, we have built the modulation curve applying a filter in the adjacency order of scattered events. In particular, as a first trial, we have selected double events whose distance between the hits is comprised between 2 and 5 pixels. The result is presented in Fig. 8, for the usual case of *Z=free* and *Z=cost*. The implementation of this event filter produces a marked improvement of both the maximum Q and the shape of the modulation curves. In the case of *Z=free* double events the maximum Q reach a value of 0.47 with respect to 0.27 for the no adjacency filter case. The improvement of maximum Q is even greater when the filter is applied to *Z=cost* double events, reaching 0.75 (0.33 for the no adjacency filter case). Of course, as it is possible to infer from the same figure, this improvement is paid also, in this case, by a dramatic loss in the statistical significance of the calculated modulation values. In fact, the 1σ errors become quite large, in particular for the *Z=cost* double events selection, decreasing drastically the reliability of the result. This improvement is mainly due to the fact that excluding the first order adjacency only a very low percentage of double events is left (see Fig. 6 - left) in particular in the direction orthogonal to the polarization plane. This tendency is confirmed if we apply an adjacency filter selecting only double events whose hits are at a distance between 3 and 6 pixels. The maximum Q again improve (0.85 for *Z=cost*), but the errors become so larger that the estimated values have almost no statistical significance.

As expected, the modulation curves exhibit a smoother and more continuous shape as function of the phase angle: the effect of the square discretization of the detector is less evident.

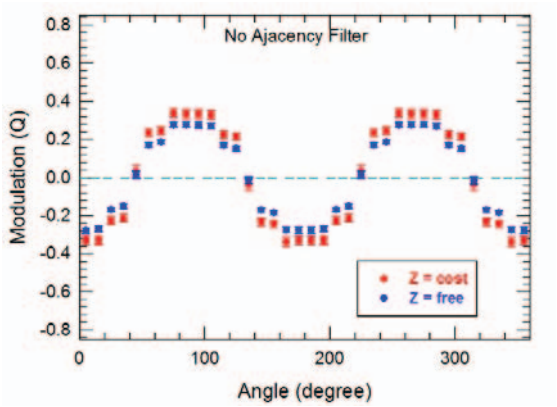

Fig. 7. The modulation curve with no adjacency filter: Q for all the double events (*z=free*) is 0.277 ± 0.015, while for the *z=cost* double event Q= 0.331 ± 0.023. This values are consistent with the ones reported in Table II.

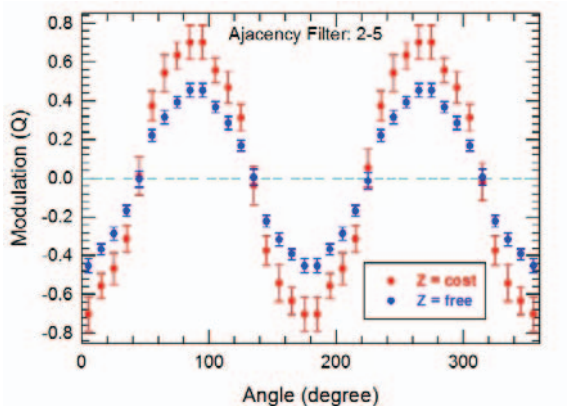

Fig. 8. The modulation curve obtained using double events with adjacency between 2 and 5, with *Z=cost* and *Z=free*, respectively. The errors are at 1σ level.

Because the significance of the results strongly depends of the events statistics, we have also implemented in the analysis tool the possibility to easily define the width of the angular aperture of the orthogonal sectors used to evaluate the N_x and

the N_y counts required for the evaluation of Q vs the phase angle (see Fig. 6-right). Increasing the amplitude of the angular aperture of these sectors, we can increase the statistics, of course loosing again in some other characteristics, like the maximum Q values and the sensitivity to phase angle. In Fig. 9 we present the modulation curves obtained with two different angle aperture of the integration sectors (5° and 10°, respectively) using double events within 2 to 5 pixel adjacencies. The doubling of the count integration area over the scattering matrix does not have any apparent effect in the quality of the Q factor. In fact, the only effect, not reported in the figure, is the increase of the statistical significance of each point in the modulation curve of $\sim\sqrt{2}$ using 10° aperture with respect to 5°. The apparent discontinuity each 45° is related with the square shape of pixels. When phase angle pass through the diagonal of pixel/detector the number of pixels that contribute to counts change suddenly and this reflects in the value of the modulation.

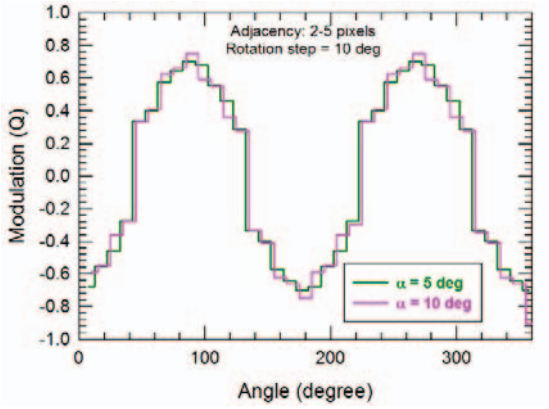

Fig. 9. Filter 2-5 adjacency order for *Z=cost* and two angle aperture of the integration section over the scattering map.

As a first conclusion, this preliminary analysis shows that a procedure to optimize the polarization response of a 3D spectrometers for each geometrical configuration should first of all determine the best tradeoff between the statistical significance and the quality of the modulation factor.

VI. On Going Activities and Perspective

The CμSP balloon borne payload is a pathfinder for future space instrumentation based on new hard X- and soft γ-rays focusing optics (Multilayer Concentrators and broad band Laue lens) or for a small satellite mission intrument.

In particular, we plan to focus future activities on the following main lines:

- Validation of the Monte Carlo code by comparison with experimental data (e.g. the ESRF results on the Caliste 256 module);
- Implementation of a model of the readout detector response (e.g. a realistic energy resolution model);
- Investigation of the effect of pixel size on the polarimetric capabilities (future space instrumentation, e.g. Laue Lens Telescope);
- Further investigation on the polarimetric performance optimization through accurate data analysis and fine-tuning of the double events selection filters.

References

[1] Weisskopf, M. C. et al., "The prospects for X-ray polarimetry and its potential use for understanding neutron stars", in Neutron Stars and Pulsars, Astrophys. Space Sci. Library, 2006, vol. 357, p. 589.

[2] Dean, A.J., et al., "Polarized Gamma-Ray Emission from the Crab", Science, vol. 321, pp. 1183 (2008).

[3] Forot, M., et al., "Polarization of the Crab pulsar and nebula as observed by the Integral/IBIS telescope", Astrophys. J., vol. 688, p. 29 (2008).

[4] Laurent, P., et al., "Polarized gamma-ray emission from the galactic black hole Cygnus X-1", Science, vol. 332, p. 438 (2011).

[5] Götz, D., et al., "GRB 140206A: the most distant polarized gamma-ray burst", Monthly Notices of the Royal Astr. Soc., vol 444, p.2776 (2014).

[6] Yonetoku, D., et al, "Magnetic Structures in Gamma-Ray Burst Jets Probed by Gamma-Ray Polarization", The Astrophys. Journal Letters, vol. 758, p. L1 (2012).

[7] Pearce, M. et al., "Balloon-borne hard X-ray polarimetry with PoGOLite", 2012 IEEE Nucl. Sci. Symp. Conf. Records, p. 1885 (2012).

[8] McConnell, M. L., et al., "Current status of the GRAPE balloon program", Proc. of SPIE 9144, Space Telescopes and Instrumentation: Ultraviolet to Gamma Ray, vol. 9144, p. 91443P (2014).

[9] Orsi, S., et al., "The POLAR gamma-ray burst polarimeter onboard the Chinese Spacelab", Proc. of SPIE 9144, Space Telescopes and Instrumentation: Ultraviolet to Gamma Ray, vol. 9144, p. 91440M (2014).

[10] M. Chauvin, et al., "Observation of polarised hard X-ray emission from the Crab by the PoGOlite Pathfinder", submitted to MNRAS (2015); arXiv:1511.02735v1 [astro-ph.IM].

[11] "Hard x-ray/soft gamma-ray telescope designs for future astrophysics missions", Proc. SPIE, Optics for EUV, X-Ray, and Gamma-Ray Astronomy VI, vol. 8861, p. 886116 (2013).

[12] F. Frontera et al., "Scientific prospects in soft gamma-ray astronomy enabled by the LAUE project", Proc. of SPIE, Optics for EUV, X-Ray, and Gamma-Ray Astronomy VI, vol. 8861, p. 886106 (2013).

[13] F. Lei, A. J. Dean, and G. L.Hills, "Compton polarimetry in gamma-ray astronomy", Space Science Review., vol. 82, p. 309 (1997).

[14] E. Caroli, et al., "A CdTe position sensitive spectrometer for hard X- and soft γ-ray polarimetry", Nucl. Instr. and Meth. in Phys. Res. A, vol. 477, pp. 567–573 (2002).

[15] Caroli, E., et al. "A Polarimetric Experiment With a Laue Lens and CZT Pixel Detector", IEEE Trans. on Nucl. Sci., vol. 56, p. 1848 (2009).

[16] Curado da Silva, R.M. et al., "Polarization Degree and Direction Angle Effects on a CdZnTe Focal Plane Performance", IEEE Trans. on Nucl. Sci., vol. 59, p. 1628 (2012).

[17] Antier, S., et al., "Hard X-ray polarimetry with Caliste, a high performance CdTe based imaging spectrometer", Experimental Astronomy, vol. 39, pp: 233–258, (2005).

[18] Gálvez, J. L., et al., "Development and Performance of a Gamma-Ray Imaging Detector", Proc. of SPIE, Ultraviolet to Gamma Ray, vol. 8443, p. 844336 (2012).

[19] Kuvvetli, et al., "A 3D CZT high resolution detector for X-and gamma-ray astronomy", Proc. of SPIE, High Energy, Optical, and Infrared Detectors for Astronomy VI, vol. 9154, p. 91540X (2014).

[20] N. Auricchio, et al., "Development status of a CZT spectrometer prototype with 3D spatial resolution for hard X ray astronomy", Proc SPIE, High Energy, Optical, and Infrared Detectors for Astronomy V, vol. 8453, p. 84530S-1 (2012).

[21] Caroli, E., et al., "A 3D CZT hard x-ray polarimeter for a balloon-borne payload", Proc. of SPIE, Space Telescopes and Instrumentation: Ultraviolet to Gamma Ray, vol. 8443, p. 84434O (2012).

[22] Allison, J. et al. "Geant4 developments and applications", IEEE Trans. on Nucl. Sci., vol. 53, p. 270 (2006). Website: http://geant4.cern.ch/

[23] MATLAB website: http://www.mathworks.com/products/matlab/